

The Vienna 4G/5G Drive-Test Dataset

Wilfried Wiedner^{1,2,*} Lukas Eller^{1,2,†} Mariam Mussbah^{1,2} Dominik Rössler^{1,2}
Valerian Maresch^{1,2} Philipp Svoboda^{1,2} Markus Rupp¹

¹Institute of Telecommunications, TU Wien, Gusshausstraße 25, 1040 Vienna, Austria

²Christian Doppler Laboratory for Digital Twin assisted AI for sustainable Radio Access Networks, TU Wien

*Corresponding Author(s): Wilfried Wiedner (wilfried.wiedner@tuwien.ac.at)

Abstract

Machine learning for mobile network analysis, planning, and optimization is often limited by the lack of large, comprehensive real-world datasets. This paper introduces the Vienna 4G/5G Drive-Test Dataset, a city-scale open dataset of georeferenced Long Term Evolution (LTE) and 5G New Radio (NR) measurements collected across Vienna, Austria. The dataset combines passive wideband scanner observations with active handset logs, providing complementary network-side and user-side views of deployed radio access networks. The measurements cover diverse urban and suburban settings and are aligned with time and location information to support consistent evaluation. For a representative subset of base stations (BSs), we provide inferred deployment descriptors, including estimated BS locations, sector azimuths, and antenna heights. The release further includes high-resolution building and terrain models, enabling geometry-conditioned learning and calibration of deterministic approaches such as ray tracing. To facilitate practical reuse, the data are organized into scanner, handset, estimated cell information, and city-model components, and the accompanying documentation describes the available fields and intended joins between them. The dataset enables reproducible benchmarking across environment-aware learning, propagation modeling, coverage analysis, and ray-tracing calibration workflows.

Keywords: 4G; 5G; LTE; NR; drive test; dataset; digital twin; ray tracing; propagation modeling

Background & Related Work

Machine learning is increasingly applied to mobile network analysis, planning, and optimization, yet progress is constrained by the limited availability of comprehensive real-world datasets. The gap is most severe for geometry- and environment-conditioned problems, including radio map estimation and coverage prediction¹, propagation modeling and calibration², ray-tracing simulation (e.g., NVIDIA Sionna RT)³, measurement-based base-station localization⁴, fingerprinting and channel charting⁵, digital network twin (DNT) construction and calibration⁶, and 5G beam-level analysis and beam management⁷.

Beyond enabling learning-based methods, modern network engineering workflows also require datasets that support reproducible benchmarking against established model-based approaches. In particular, propagation analysis and deterministic modeling (e.g., ray tracing) rely on calibration measurements together with explicit deployment descriptors and detailed 3D environmental context. Datasets that pair real-world measurements with both cell metadata and building/terrain information

[†]This work was conducted while Lukas Eller was with the Institute of Telecommunications, TU Wien, Austria. He is now with Huawei Technologies, Munich, Germany.

therefore provide a strong foundation for benchmarks spanning artificial intelligence (AI)-based and traditional methods, including environment-aware learning and digital twin (DT) calibration.

Several open measurement datasets have recently been released, providing valuable empirical evidence on 4G/5G coverage and performance across different cities and scenarios^{8–10}. However, these datasets typically focus on measurement traces and key performance indicators (KPIs), and do not jointly provide explicit deployment descriptors together with detailed building/terrain context.

Complementing these real-world measurement efforts, Yapar *et al.*¹¹ propose a synthetic dataset of pathloss and time-of-arrival maps generated via ray tracing on OpenStreetMap-based city models. While it incorporates detailed building and terrain geometry and is well suited for propagation-modeling studies, its ray-traced nature may not fully capture the complexity of real operator deployments or measured network performance.

A more recent ray-tracing-based benchmark for radio-map learning is introduced in Jaensch *et al.*¹², offering a large collection of simulated radio maps alongside map-derived features such as directional transmitter antennas and environment descriptors derived from building-height and vegetation models. While valuable for benchmarking radio-map estimation methods, it remains entirely synthetic and likewise lacks real operator deployments and measurement-based validation; indeed, comparisons between ray-tracing simulations and field measurements can show substantial discrepancies¹³.

More recent large-scale empirical datasets have further expanded the landscape of open mobile network measurements, including multi-campaign collections for Long Term Evolution (LTE) and 5G New Radio (NR) analysis and rich drive-test datasets aimed at quality-of-service (QoS) prediction and mobility-aware modeling^{14,15}. While these datasets significantly enrich the ecosystem of open mobile network data, they still focus primarily on performance metrics and mobility traces rather than on the explicit integration of deployment descriptors and high-resolution environmental information.

Among the existing open datasets, the *DoNext* dataset¹⁶ represents the closest empirical point of comparison to the dataset presented in this work. DoNext comprises a large-scale collection of 4G and 5G measurements from Dortmund, Germany, covering mobile, static, and rail-based campaigns over a period of two years. While it provides extensive active and passive measurements and estimated base station (BS) assignments, it does not include explicit cell deployment information or high-resolution environmental data such as terrain and building models.

Taken together, these efforts demonstrate substantial progress toward open mobile network benchmarking. However, large-scale datasets that jointly combine *real-world* measurements with deployment descriptors and high-resolution building/terrain context remain scarce—despite being central to environment-aware modeling and DT construction. To close this gap, we present the Vienna 4G/5G Drive-Test Dataset, a large-scale open-access resource that combines city-wide drive-test measurements with inferred deployment descriptors and a building/terrain model of Vienna. [Table 1](#) situates the Vienna 4G/5G Drive-Test Dataset within the landscape of publicly available datasets, comparing modality, scale, and available context. Below, we summarize the dataset contents and representative use cases it enables, including systematic evaluation and benchmarking.

The Vienna 4G/5G Drive-Test Dataset at a glance.

- **Scale and diversity:** city-wide drive-test measurements with dense geospatial sampling across suburban and urban areas.
- **Dual modality:** passive scanner + active handset logs (network-side + user-side).
- **3D environmental context:** building and terrain models enabling environment-aware workflows.

Table 1: Comparison of publicly available datasets. Digital twin readiness refers to the joint availability of deployment metadata (e.g., BS positions, orientations) and environmental context (e.g., buildings, terrain). Multi-MNO indicates measurements from multiple mobile network operators (MNOs); A+P denotes active and passive collection.

Dataset	Type 4G/5G	Multi- MNO	Active/ Passive	Scale	Digital Twin
Rochman <i>et al.</i> ⁸	✓/✓	✓	Active	2 Cities, Highway	✗
Kousias <i>et al.</i> ⁹	✓/✓	✓	A+P	City	✗
Farthofer <i>et al.</i> ¹⁰	✓/✓	✗	Active	Highway	✗
Yapar <i>et al.</i> ¹¹	Synthetic	–	–	City	Env. only
Jaensch <i>et al.</i> ¹²	Synthetic	–	–	City	Env. only
Miekkala <i>et al.</i> ¹⁵	✓/✓	✗	Active	Cities, Borders	✗
<i>DoNext</i> ¹⁶	✓/✓	✓	A+P	City	✗
Vienna 4G/5G (This work)	✓/✓	✓	A+P	City	✓ (net+env)

- **Deployment descriptors:** for a subset of sites, we provide estimated site locations, sector azimuths, and antenna heights, enabling deployment-aware analyses.
- **LTE and 5G NR (NSA):** consistent KPI set across radio access technologies (RATs), including NR beam-level measurements for benchmarking and beam-management studies.

Figs. 1–4 provide representative examples of the dataset components summarized above.

Representative evaluation tasks and benchmarking use cases enabled by the Vienna 4G/5G Drive-Test Dataset.

- **Ray-tracing calibration and benchmarking:** use measured links together with deployment descriptors and 3D building/terrain context to calibrate deterministic simulators and benchmark ray-tracing predictions against real-world observations.
- **Environment-aware radio map learning:** train and evaluate geometry-conditioned models using building/terrain features, and compare against classical and deterministic baselines.
- **Deployment inference and validation:** study site localization and sector-parameter estimation (e.g., azimuth/height) from measurement fingerprints and inferred deployment descriptors.
- **Beam-management studies:** evaluate NR beam selection and tracking under mobility using beam-level measurements.
- **Digital twin prototyping and calibration:** combine deployment metadata, 3D city model, and measurements for city-scale DT workflows.

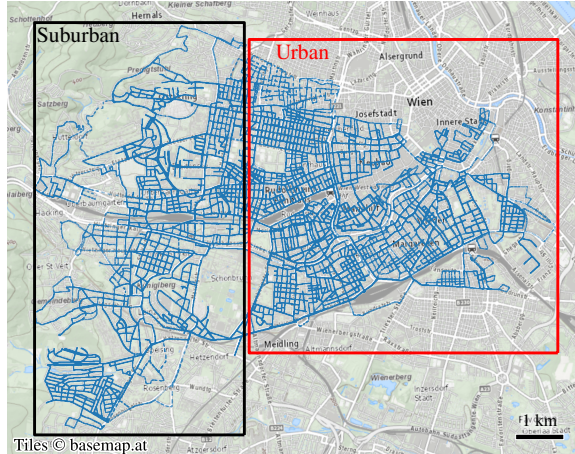


Figure 1: City-wide measurement coverage with dense sampling across suburban and urban areas (indicated by the black and red boxes).

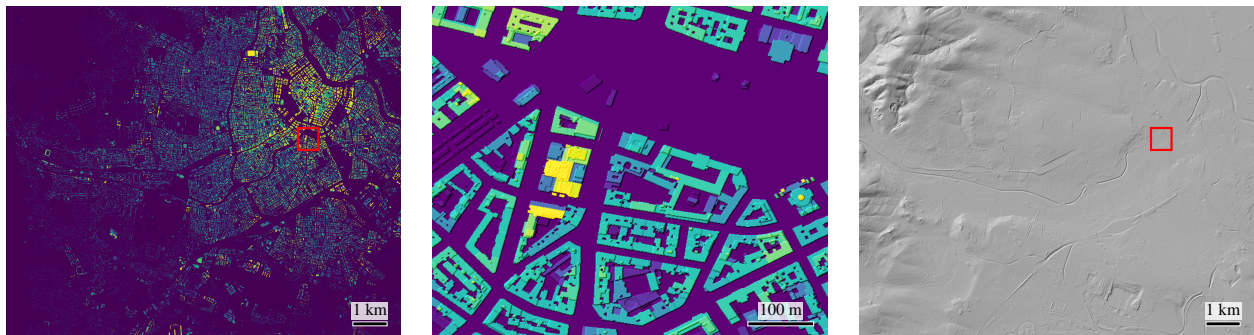


Figure 2: Overview of the city-model provided with the dataset: building model (left), a zoomed-in building-region of interest (center, indicated by the red box), and terrain model overview (right).

Methods

The dataset was collected between March 2024 and March 2025 and covers approximately 100 km^2 of Vienna, spanning both urban and suburban environments. Passive measurements were performed using a PCTEL IBflex scanning receiver (i), two OmniLOG PRO omnidirectional antennas (ii) mounted on the car rooftop, and a PCTEL Global Positioning System (GPS) receiver (iii), as illustrated in Figure 5. The scanner was connected to a notebook running Nemo Outdoor software from Keysight (Figure 5), which was used to control the measurement process and record the data. This setup enabled wideband, technology-agnostic monitoring of cellular signals with spatial diversity, providing an unbiased view of the deployed networks across the measurement area.

In parallel, active phone measurements were performed using three 5G-capable smartphones mounted on the vehicle dashboard and connected to Nemo Outdoor, capturing radio-quality metrics such as reference signal received power (RSRP), reference signal received quality (RSRQ), received signal strength indicator (RSSI), and signal-to-interference-plus-noise ratio (SINR), as well as user-centric performance indicators including throughput and timing advance (TA).

At each georeferenced measurement point (measurement ID/timestamp + GPS position), the dataset records one or more cell observations together with their identifiers—most notably PCI and channel number (and, where available, cell/BS/sector IDs)—and radio-layer KPIs. Scanner logs

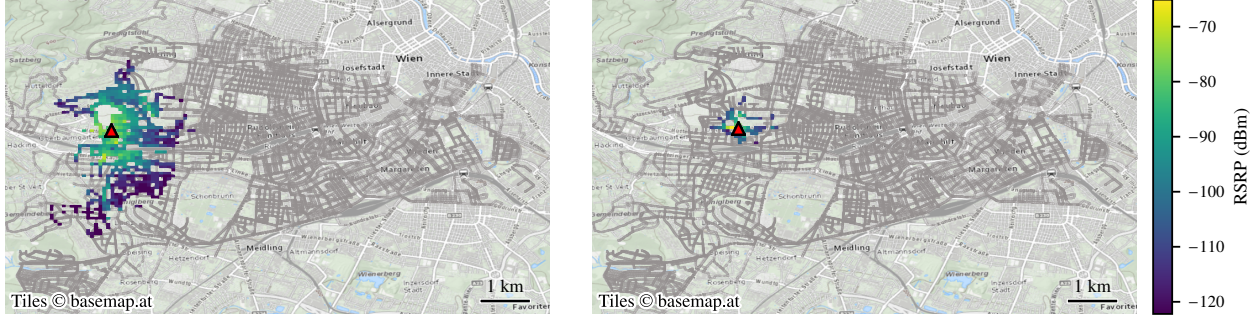


Figure 3: Example RSRP coverage maps around two BSs with different antenna heights: 38 m (left) and 19 m (right). The red triangle marks the estimated BS position; colors show RSRP.

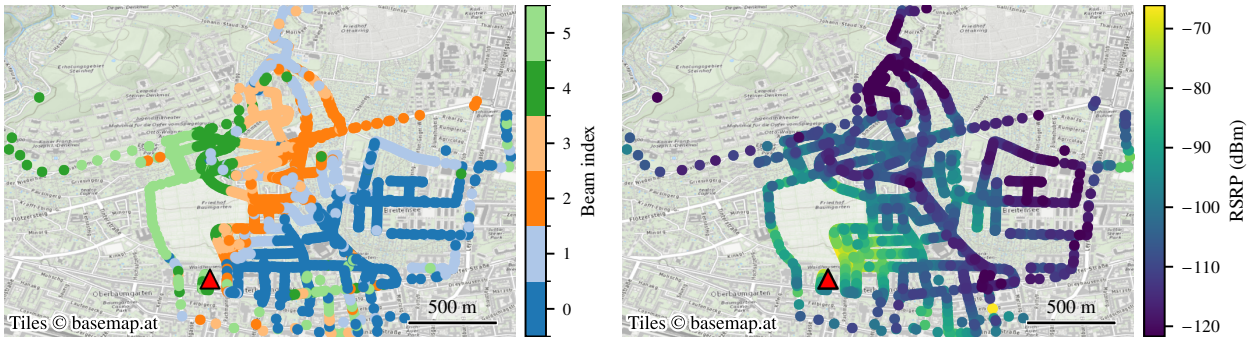


Figure 4: Example NR beam-level view for a single cell of the corresponding BS: strongest beam index per location (left) and the corresponding RSRP (right). The BS position is marked by a red triangle.

provide passive multi-cell (and for NR, beam-level) observations, whereas phone logs primarily report serving-cell measurements and add user-centric fields such as throughput and TA; in non-standalone (NSA) 5G NR phone logs, physical NR cell/gNB identifiers are not exposed (optional dataset-internal dummy IDs may be provided).

Scanner Data Processing

Post-processing followed two parallel pipelines for scanner and phone data. For the scanner measurements, raw Nemo outputs were parsed to identify master information block (MIB) and system information block (SIB) decoding events, as well as cell-specific reference signal (CRS) and synchronization signal block (SSB) events. Multi-valued records containing several physical cell identifiers (PCIs), channels, or beams were exploded into individual entries, standardized, and cleaned by filtering incomplete data.

CRS and SSB measurements were subsequently merged with the corresponding MIB and SIB information by first identifying candidate pairs via exact keys (PCI, channel, file) and then resolving ambiguities through temporal alignment and spatial filtering. The resulting records were enriched with deployment metadata such as eNodeB (eNB) ID and sector ID (LTE).

Raw Nemo logs contain hundreds of parameters in nested and multi-valued formats, with partially overlapping but RAT-specific structures. We therefore provide harmonized, analysis-ready scanner tables that expose a consistent set of scanner-side measurements (CRS/SSB events with associated MIB/SIB context) and preserve temporal and spatial alignment at scale.



Figure 5: Equipment for passive measurements (left) consisting of scanner (i), two OmniLOG PRO antennas (ii), and a GPS receiver (iii). Scanner setup in the car (right)

Phone Data Processing

For the phone data, post-processing focused on LTE primary cells (PCell) and NR serving primary secondary cells (SpCell), which form the basis of all handset-based measurements in the released dataset. A harmonized subset of key measurements—RSRP, RSRQ, RSSI, SINR, throughput, and TA—was extracted to ensure consistency across records. In the current release, handset-based 5G NR measurements in the phone data table are available for one operator only.

TA values are reported less frequently than radio-quality indicators, and not every measurement record contains a valid TA entry. To prepare TA for downstream use, duplicate timestamps were merged, missing coordinates interpolated, and invalid values discarded. The resulting TA records were then matched with the corresponding PCell or SpCell measurements based on PCI and channel number, selecting the closest spatial candidates to ensure temporal and spatial consistency. These TA-based records form the basis for the base-station location estimates reported in this work. A more detailed dataset containing additional cell types (e.g., neighbor cells and secondary cells) can be made available upon request for advanced analyses.

Base Station Estimation and Digital Network Twin Construction

To support the creation of a DNT, the locations of a representative subset of BSs were estimated for each radio access technology (RAT) and operator using the methodology of Eller *et al.*⁴. Public BS entries from the Austrian Senderkataster¹⁷ were used to constrain the search space, ensuring that only physically plausible candidate sites were considered. Antenna heights were subsequently estimated using Google Earth Pro.

For LTE, the selection of BSs was performed on a per-day basis by identifying the ten most frequently observed BSs per operator for each measurement day. This resulted in 50 distinct LTE BSs per operator across the full measurement campaign. This strategy was chosen to ensure broader spatial and temporal coverage of the network, rather than concentrating the estimation on a small number of persistently dominant sites. As LTE measurements include network-reported cell identifiers, measurements could be directly grouped by BS prior to location estimation.

For 5G NR measurements, the handset logs collected in NSA mode do not expose physical NR

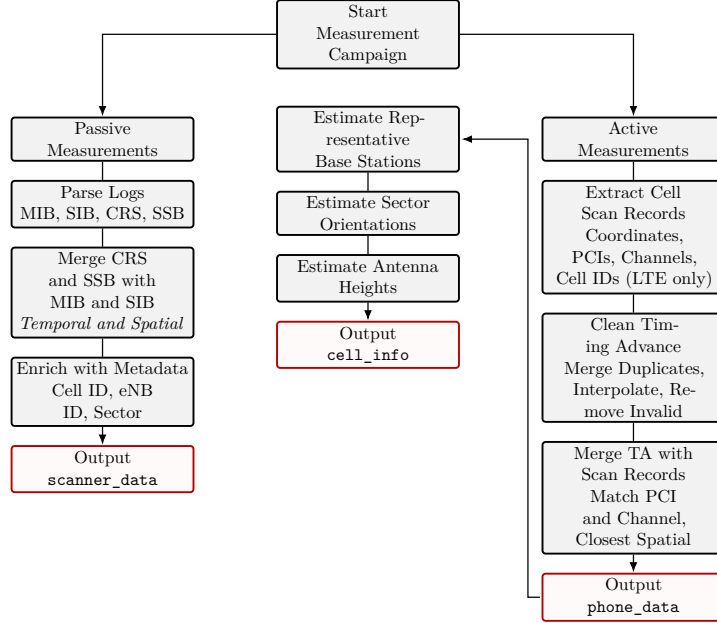


Figure 6: Illustration of the data collection and processing pipeline.

cell or gNodeB (gNB) identifiers, which prevents direct grouping of measurements belonging to a specific BS. To address this limitation, we adopt a PCI-based grouping heuristic. Specifically, we assume that within a single measurement day a given NR PCI is not reused across different gNBs, which is reasonable in our setting given the limited geographic coverage per day and the typically large NR PCI space. Based on this assumption, the thirty most frequently observed PCIs per measurement day were selected, subject to the additional requirement that each PCI be represented by at least five measurement samples acquired at distinct locations.

Prior to BS localization, spatial consistency was assessed for each selected PCI by constructing TA circles centered at the corresponding user equipment (UE) measurement locations, with the TA value defining the circle radius. The overlap of these circles was evaluated to determine whether the measurements could plausibly originate from a common transmitter location. In cases where the TA circles associated with the same PCI formed disjoint spatial subsets—indicating multiple spatially inconsistent transmitter hypotheses—only the subset containing the largest number of samples was retained for subsequent BS location estimation. This procedure ensures that the localization step is applied only to the most spatially consistent and well-supported measurement cluster. Due to data availability constraints, this 5G NR cell estimation procedure is currently applied for one network operator only.

Finally, sector orientations were estimated using handset-based measurements. For each estimated BS, the RSRP-weighted centroid of the associated phone measurement locations was computed, and the azimuth from the estimated BS position to this centroid was calculated. An azimuth of 0° corresponds to geographic north, with angles increasing clockwise, consistent with standard cartographic and navigation conventions^{18,19}. Phone measurements were used for sector orientation estimation to ensure methodological consistency with the timing-advance-based localization process and to avoid ambiguities arising from beam- or snapshot-level scanner observations.

The overall data collection and processing chain is illustrated in Figure 6, where TA is depicted as the representative phone-side performance indicator; the released dataset additionally includes RSRP, RSRQ, RSSI, SINR, and throughput.

Technical Validation

This section summarizes the validation analyses performed to assess the reliability and accuracy of the Vienna 4G/5G Dataset. The focus lies on aspects that are essential for downstream use in research, simulation, and data-driven modeling, namely the spatial accuracy of the recorded measurement locations, the consistency of cell assignments in the scanner data, and the statistical properties of KPIs such as RSRP and RSRQ. In addition, the specifications and accuracy limits of the employed measurement equipment are summarized to provide context for the achievable precision of the recorded data. Where appropriate, residual distributions, box plots, and summary tables are used to illustrate errors and variances observed in the dataset.

Georeferencing Accuracy

All measurement locations in the released dataset are stored as raw GPS records in geographic coordinates (EPSG:4326, latitude and longitude). For distance-based analyses, such as spatial error evaluation or map-based snapping, reprojection to a metric coordinate reference system is required; in this work, EPSG:31287 was used. The reprojected coordinates are not included in the dataset itself, but all positioning accuracy results reported in this section were obtained after reprojection.

GPS measurements are subject to noise, particularly in dense urban environments with limited satellite visibility, and recorded positions may deviate from the actual road geometry. To quantify this effect, GPS samples were compared to the nearest street segments extracted from OpenStreetMap. Let $p_i \in \mathbb{R}^2$ denote a reprojected GPS point and let \mathcal{S} be the set of street polylines. The snapped point and corresponding lateral offset are defined as

$$s(p_i) = \arg \min_{q \in \mathcal{S}} \|p_i - q\|_2,$$
$$d_i = \|p_i - s(p_i)\|_2.$$

The overall positioning error was evaluated using the root mean square error (RMSE),

$$\text{RMSE} = \sqrt{\frac{1}{N} \sum_{i=1}^N d_i^2},$$

where d_i denotes the per-sample horizontal offset and N is the total number of samples.

Applied to the Vienna 4G/5G Dataset, this analysis yields an RMSE of approximately 4 m. This value is consistent with expected GPS accuracy under urban driving conditions and confirms that the recorded locations provide sufficient spatial precision for drive-test-based propagation analysis and BS localization. A representative example illustrating raw GPS samples, snapped positions, and the corresponding correction vectors is shown in [Figure 7](#).

Cell Assignment Consistency

The consistency of assigning physical-layer scanner measurements to broadcast system information was evaluated by analyzing temporal and spatial residuals between CRS and SSB records and their MIB and SIB decoding events. This analysis provides an internal validation of the scanner parsing and enrichment pipeline.

Candidate assignments were identified based on exact matching keys (PCI, channel number, measurement file) and subsequently evaluated using temporal and spatial consistency criteria. The

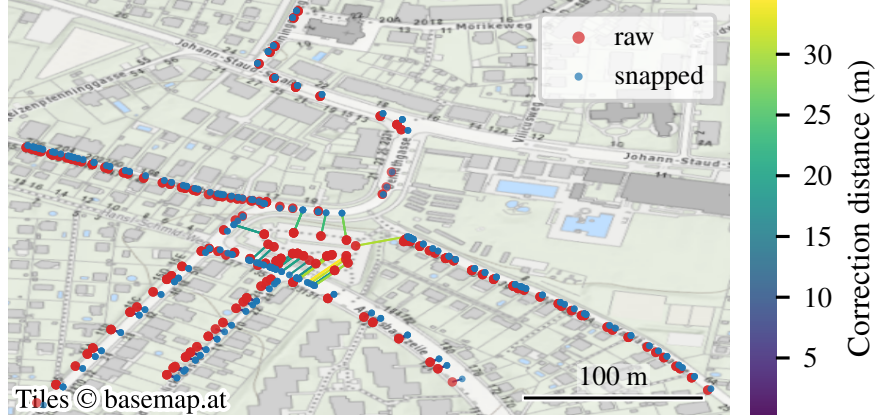


Figure 7: Example of GPS samples (red) snapped to the nearest road (blue) with correction vectors (colored lines). The line color encodes the correction distance in meters.

Table 2: CRS/SSB to MIB/SIB assignment outcomes split by technology: counts of matched and unmatched records. Matched includes ok, time-outlier, and space-outlier.

Technology	N total	Matched (any)	Unmatched
Overall	2,649,377	2,176,732	472,645
LTE	655,310	557,668	97,642
5G NR	1,994,067	1,619,064	375,003

nominal acceptance set was defined as

$$\mathcal{A} = \{(i, j) : |\Delta t_{ij}| \leq \tau_t \wedge \Delta x_{ij} \leq \tau_x\},$$

$$\tau_t = 10 \text{ s}, \quad \tau_x = 750 \text{ m},$$

where Δt_{ij} denotes the timestamp difference between a CRS/SSB detection and a MIB/SIB decoding event, and Δx_{ij} the corresponding point-to-point distance evaluated in EPSG:31287.

Each CRS/SSB record is linked to at most one candidate MIB/SIB event. Records with at least one candidate (i.e., at least one event sharing the exact matching keys PCI, channel number, and measurement file) are classified as ok if both criteria are satisfied, or as time-outlier and/or space-outlier if the temporal and/or spatial criterion is violated. Records with no candidate under the exact-key match are labeled unmatched. For compactness, [Table 2](#) reports matched vs. unmatched counts, where matched includes ok and any outlier case (including violations of both criteria). [Table 3](#) reports the percentages of time-outlier, space-outlier, and unmatched samples; the fraction of ok samples equals 100% minus the reported percentages.

Across the full dataset, 2,649,377 CRS/SSB records were evaluated, of which 472,645 (17.84%) could not be matched to a corresponding MIB/SIB decoding event. In LTE, 655,310 records were processed, with 14.90% unmatched, whereas in 5G NR, 1,994,067 records were evaluated, with 18.81% unmatched.

Temporal residuals exhibit a pronounced long tail,

$$\text{median } |\Delta t| = 0 \text{ s},$$

$$P_{90} = 2030 \text{ s}, \quad P_{95} = 4585 \text{ s}, \quad P_{99} = 14\,763 \text{ s},$$

Table 3: CRS/SSB to MIB/SIB assignment outcomes split by technology: percentages of time-outlier, space-outlier, and unmatched records. The fraction of ok samples equals 100 % minus the reported percentages.

Technology	Time-outlier [%]	Space-outlier [%]	Unmatched [%]
Overall	13.84	0.53	17.84
LTE	17.99	1.96	14.90
5G NR	12.48	0.06	18.81

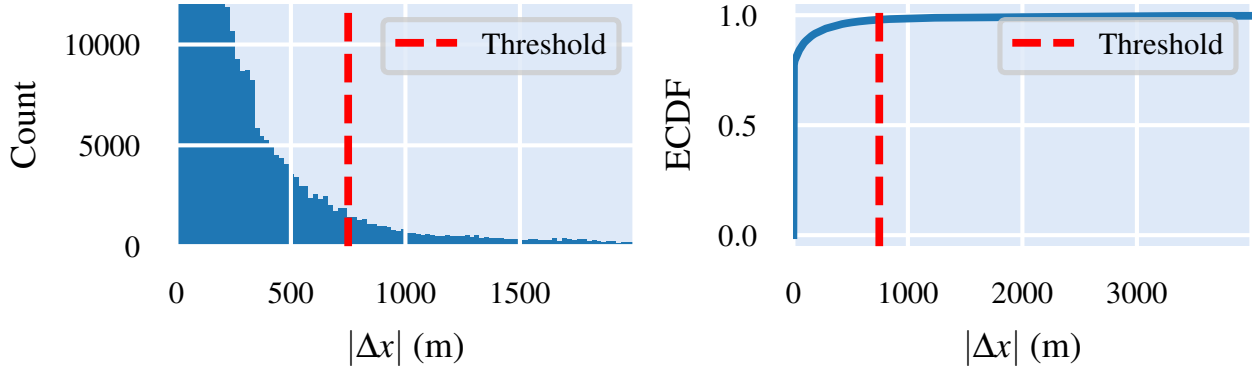


Figure 8: Spatial residuals for CRS/SSB to MIB/SIB assignment. Histogram (clipped at 12 000) and empirical CDF of $|\Delta\mathbf{x}|$. The dashed vertical line denotes the acceptance threshold $\tau_x = 750$ m.

reflecting asynchronous decoding behavior and buffering effects in the scanner logs. In contrast, spatial residuals are considerably tighter (Figure 8),

$$\begin{aligned} \text{median } |\Delta x| &= 0 \text{ m}, \\ P_{90} &= 145 \text{ m}, \quad P_{95} = 342 \text{ m}, \quad P_{99} = 1423 \text{ m}. \end{aligned}$$

Because the nominal temporal threshold $\tau_t = 10$ s proved too restrictive given the observed jitter, the released dataset relies on a spatial fallback strategy. For each CRS/SSB record i , the MIB/SIB record j^* that minimizes the spatial residual is selected,

$$j^*(i) = \arg \min_{j \in \mathcal{C}(i)} \Delta x_{ij} \quad \text{s.t.} \quad \Delta x_{ij} \leq \tau_x,$$

where $\mathcal{C}(i)$ denotes the set of candidate MIB/SIB decoding events consistent with the CRS/SSB key tuple. Temporal residual statistics are nevertheless reported for transparency and may inform alternative threshold choices in downstream analyses (Figure 9).

Key Performance Indicator Statistics

The distributions of RSRP and RSRQ derived from the scanner-based measurements across the available LTE and NR carriers are summarized in Figure 10. As expected, the LTE 800 MHz low-band carrier (B20) exhibits the strongest received power, reflecting favorable propagation conditions at lower frequencies. Mid-band LTE 1800 MHz (B3) and 2600 MHz (B7) show progressively lower RSRP levels, while the NR 3500 MHz C-band (n78) displays the weakest received power due to increased path loss and reduced building penetration. The NR 2100 MHz carrier (n1) exhibits intermediate behavior, consistent with its frequency range.

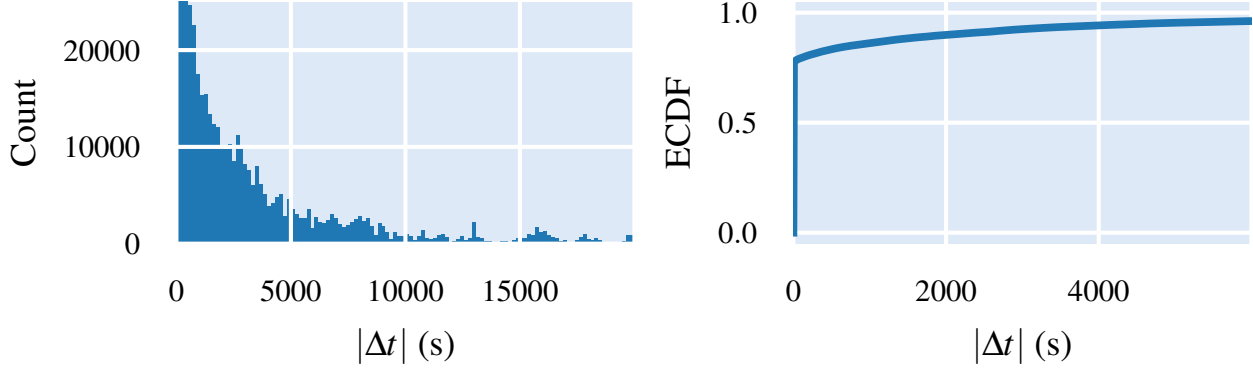


Figure 9: Temporal residuals for CRS/SSB to MIB/SIB assignment. Histogram (clipped at 25 000) of $|\Delta t|$ and ECDF of $|\Delta t|$.

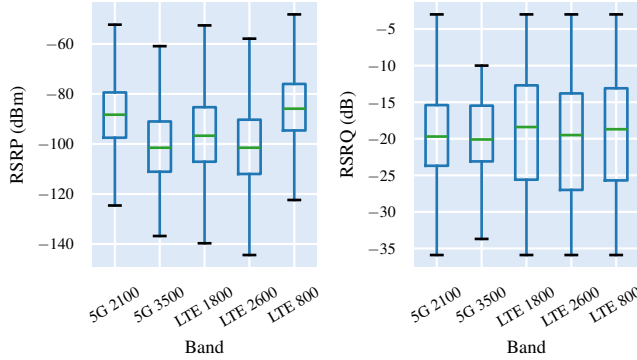


Figure 10: Distributions of RSRP and RSRQ across LTE and NR carriers. Boxplots are grouped by carrier frequency: LTE 800 MHz (B20), LTE 1800 MHz (B3), LTE 2600 MHz (B7), NR 2100 MHz (n1), and NR 3500 MHz (n78).

In terms of RSRQ, low-band LTE again provides the most stable quality values, with median levels close to -9 dB. Mid- and high-band layers show a wider dispersion of RSRQ, attributable to higher cell density and increased interference. Overall, these band-dependent differences confirm that the scanner measurements capture realistic propagation and interference characteristics across heterogeneous spectrum deployments.

Plausibility and Validation of Estimated Base Station Metadata

To support the creation of a DNT, a subset of BSs was localized using timing-advance-based methods. For LTE, where network-reported cell identifiers enable unambiguous grouping and reference metadata are available for part of the deployment, the estimated BS locations and sector orientations were quantitatively assessed.

Localization accuracy was evaluated using the RMSE between estimated and reference BS positions, while sector orientations were assessed using the mean absolute circular error between estimated and reference azimuth angles. Across the validated LTE sites, a localization RMSE of 38.55 m and a mean absolute circular error of 27.95° were observed, indicating a physically consistent and plausible reconstruction of the underlying deployment.

For 5G NR, handset-based measurements were collected in NSA mode, where physical NR cell

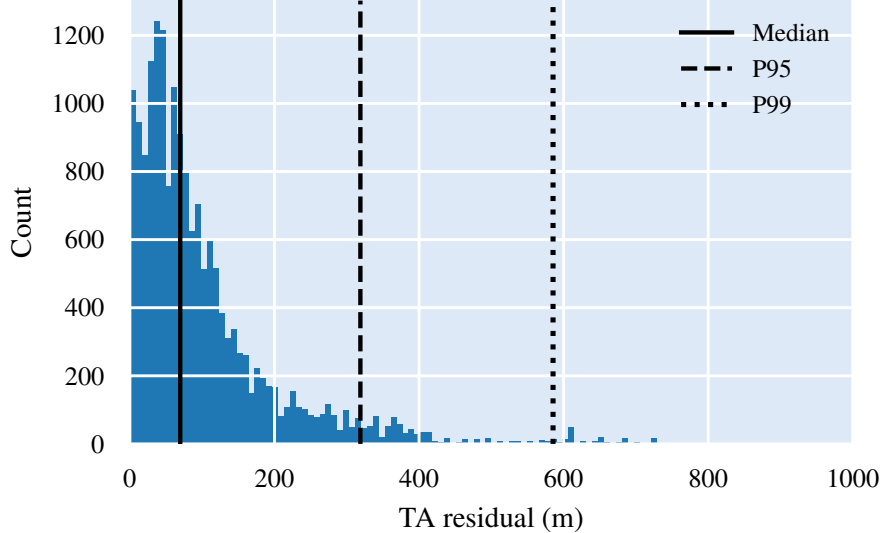


Figure 11: Timing-advance residual distribution for 5G NR. Vertical lines indicate the median, 95th percentile, and 99th percentile of the residuals. For clarity, the horizontal axis is limited to 1000 m.

or gNB identifiers are not exposed by commercial devices. As a result, measurements cannot be grouped unambiguously by base station, and external reference metadata are not available for direct quantitative validation. Consequently, the assessment of estimated 5G BS metadata is limited to internal consistency and plausibility checks.

TA consistency was evaluated by comparing the TA-derived range to the geometric distance between each UE measurement position and the corresponding estimated BS location. With an NR TA step size of $1 \text{ TA} = 1.2216 \text{ m}$, the per-sample residual is defined as

$$r_i = \left| \|\mathbf{x}_i - \hat{\mathbf{b}}\|_2 - 1.2216 \cdot \text{TA}_i \right|,$$

where \mathbf{x}_i denotes the UE position and $\hat{\mathbf{b}}$ the estimated BS position. As shown in Figure 11, the resulting residual distribution exhibits a median of 69.6 m with $P_{95} = 318.8 \text{ m}$ and $P_{99} = 585.4 \text{ m}$ across $N = 17,433$ NR samples, indicating that the inferred 5G locations remain compatible with the underlying TA constraints.

Scanner Specifications

Passive measurements were collected using a PCTEL IBflex scanning receiver connected to two OmniLOG PRO omnidirectional antennas and a dedicated GPS receiver. Table 4 summarizes the key specifications that are relevant for interpreting the dataset accuracy. Further details are available in the manufacturer’s datasheet²⁰. The commercial handsets used for phone-based measurements are treated as representative user equipment rather than calibrated measurement instruments; detailed device information is provided in the dataset documentation.

Data Record

The Vienna 4G/5G Drive-Test Dataset is archived on Zenodo under a concept DOI ([10.5281/zenodo.18322065](https://doi.org/10.5281/zenodo.18322065)), which resolves to all released versions, including future updates. This descriptor

Table 4: Scanner measurement specifications for LTE and 5G NR modes

	Specification	
	LTE	NR
Measurement mode	Synchronization channels	
Reported data	PCI, RSRP, RSRQ, CINR (LTE), SINR (NR), delay spread, time, latitude, longitude; NR additionally: beam index	
Max. number of PCI	16	8 (max. 8 beams/PCI)
Subcarrier spacing	15 kHz	15/30 kHz
Minimum detection level	-140 dBm	-135 dBm
Accuracy (CINR/SINR)	± 1 dB	± 2 dB
Measurement rate (typical)	50 s^{-1}	30 s^{-1}

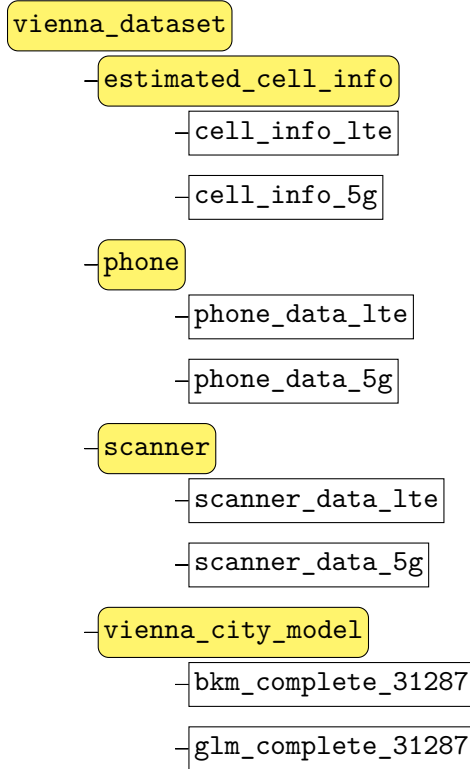


Figure 12: Directory structure of the Vienna 4G/5G Dataset.

and all results reported in this paper are based on dataset version 3 (versioned DOI: [10.5281/zenodo.18338399](https://doi.org/10.5281/zenodo.18338399)). For reproducibility, we recommend citing the versioned DOI when referring to this release, and the concept DOI when referring to the dataset in general.

As illustrated in Figure 12, the Vienna 4G/5G Dataset is organized into four main subdirectories: (i) estimated cell information, (ii) phone measurements, (iii) scanner measurements, and (iv) the

Table 5: Common metadata fields across all measurement types.

Column	Type	Unit	Description
operator	String	–	Mobile network operator identifier (A, B, or C)
channel_number	Integer	–	Radio frequency channel number
frequency_khz	Integer	kHz	Carrier center frequency
pci	Integer	–	Physical Cell Identity
cell_id	Integer	–	Unique cell identifier (LTE and NR where available)
enb_id / gnb_id	Integer	–	BS identifier (LTE/NR where available)
cell_id_dummy	Integer	–	Auxiliary dataset-internal cell identifier (NR only, where available)
gnb_id_dummy	Integer	–	Auxiliary dataset-internal gNB identifier (NR only, where available)
sector_id	Integer	–	Sector identifier within the site
timestamp / time	datetime	–	Measurement time in UTC (<code>datetime64[ns]</code>)
latitude	Float	deg	Geographic latitude (EPSG:4326)
longitude	Float	deg	Geographic longitude (EPSG:4326)

Vienna city model. Measurement and metadata files are provided in CSV and Parquet formats, while terrain and building models are distributed as GeoTIFF rasters. The combination of estimated cell metadata (BS locations, antenna heights, and sector azimuths) with the high-resolution city model enables environment-aware analyses and learning workflows, such as training propagation surrogates and supporting AI-assisted network planning. The following subsections describe the contents and available columns in each subdirectory. Complementary technical notes and ancillary information are available in the associated repository.

Common Metadata and Identifiers

Several identifiers are used to enable spatial, temporal, and operator-level alignment between measurement records and estimated cell metadata. These fields are shared across scanner and phone measurements and are summarized in [Table 5](#). They enable merging per-sample measurements with per-cell metadata, which is essential for environment-aware propagation learning and planning-oriented machine learning models.

For LTE, standardized network-reported identifiers (`cell_id`, `enb_id`, `sector_id`) are available and used directly throughout the dataset. For 5G NR measurements collected in NSA mode, physical NR cell and gNB (5G BS) identifiers are not exposed by commercial handsets. In such cases, auxiliary dataset-internal identifiers (`cell_id_dummy` and `gnb_id_dummy`) are provided where reliable cell estimates are available.

These auxiliary identifiers do not correspond to standardized 3GPP identifiers. They serve exclusively as stable internal keys to enable grouping of NR measurements and linkage to estimated NR cell metadata. Their presence is optional, and the corresponding fields may be null for NR measurements where no cell estimates exist.

Table 6: Radio-layer signal and quality indicators.

Column	Type	Unit	Description
rsrp_dbm	Float	dBm	Reference Signal Received Power (RSRP)
rsrq_db	Float	dB	Reference Signal Received Quality (RSRQ)
rsqi_dbm	Float	dBm	Received Signal Strength Indicator (RSSI)
sinr_db	Float	dB	Signal-to-Interference-plus-Noise Ratio (SINR); reported for phone measurements and NR scanner measurements.
cinr_db	Float	dB	Carrier-to-Interference-plus-Noise Ratio (CINR); reported for LTE scanner measurements only.
pathloss_db	Float	dB	Path loss estimated from transmit reference power

Table 7: Source-specific and RAT-specific fields.

Column	Applies to	Type	Unit	Description
beam_index, beam_type	5G NR only	Integer, String	–	Beam index and type (Serving or Detected).
dl_throughput_mbps	Phone only	Float	Mbit/s	Downlink user throughput.
ul_throughput_mbps	Phone only	Float	Mbit/s	Uplink user throughput.
timing_advance	Phone only	Integer	–	Timing advance (round-trip delay indicator).

Radio-Layer Metrics

In addition to these identifiers, all measurement datasets (scanner and phone) include physical-layer signal and quality indicators. These metrics are defined consistently across LTE and NR where applicable and are summarized in [Table 6](#).

Note: CINR is reported only for LTE scanner measurements. All other signal-quality ratio values are stored as SINR (`sinr_db`).

Finally, [Table 7](#) summarizes additional fields that are specific to either the measurement source (scanner vs. phone) or the RAT (LTE vs. NR). These include user throughput, timing advance, and NR beam-level information.

Estimated Cell Information

This subdirectory provides metadata for LTE and 5G NR cells estimated from decoded broadcast information, public deployment registers, and measurement-based geolocation. Each record represents one estimated cell or sector and includes stable identifiers, carrier frequency information, geographic location, and sector configuration parameters such as antenna azimuth and height.

Where standardized network-reported identifiers are unavailable (i.e., for NR measurements collected in NSA mode), auxiliary dataset-internal identifiers are used to enable consistent grouping of measurements and linkage to the corresponding estimated cell metadata. Azimuth angles follow the geographic convention, with 0° corresponding to north and positive values counted clockwise. The available columns are summarized in [Table 8](#).

The use of consistent column naming and units facilitates merging cell information with corresponding scanner and phone measurements, enabling spatially and temporally aligned analyses of

Table 8: Columns of the estimated cell information files.

Column	Type	Unit	Description
technology	String	–	Radio access technology (LTE or NR)
enb_id	Integer	–	eNodeB identifier of the site (LTE)
sector_id	Integer	–	Sector identifier within the site
cell_id	Integer	–	Unique cell identifier (LTE)
cell_id_dummy	Integer	–	Auxiliary dataset-internal NR cell identifier
gnb_id_dummy	Integer	–	Auxiliary dataset-internal gNB identifier
pci	Integer	–	Physical Cell Identity
channel_number	Integer	–	Radio frequency channel number
latitude	Float	deg	BS latitude (EPSG:4326)
longitude	Float	deg	BS longitude (EPSG:4326)
height_m	Integer	m	Antenna height above ground level
azimuth_deg	Integer	deg	Antenna azimuth orientation

both coverage and performance.

Vienna City Model

This subdirectory provides environmental data forming the basis of the Vienna DNT. It includes the Building Model (BKM) and Ground-Level Model (GLM), both stored as GeoTIFF rasters in EPSG:31287 and compressed using 7-Zip. Both rasters provide height information at 1 m spatial resolution, representing building heights and terrain elevation, respectively. Together, these layers enable environment-aware analyses and learning tasks such as (i) training propagation surrogates conditioned on local urban morphology, (ii) learning blockage- and diffraction-aware coverage models, or (iii) supporting AI-assisted network planning pipelines that combine cell metadata with 3D urban context.

Usage Notes

All timestamps in the dataset are stored as `datetime64[ns]` values without explicit timezone information and are expressed in Coordinated Universal Time (UTC). Users working with local time representations should apply the appropriate timezone conversion if required for visualization or interpretation.

Measurement files containing spatial information include raw GPS coordinates in EPSG:4326. For distance-based analyses, it is recommended to transform the data to a metric coordinate reference system, such as EPSG:31287. To improve spatial consistency in map-based analyses, users may optionally snap measurement locations to the nearest street segments; however, the dataset itself does not apply any map-matching or spatial correction.

All handset 5G NR measurements (phone data) in this dataset were collected in NSA mode, with LTE serving as the primary connection. As a result, physical NR cell identifiers (i.e., `cell_id`, `gnb_id`, `sector_id`) are not reported by the handset logging interface and are therefore not present in the NR phone traces. Only LTE anchor cell identifiers are available in the phone dataset. NR and

LTE samples can be temporally aligned to associate each NR measurement with its corresponding LTE anchor, enabling joint LTE–NR analyses at the connection level.

Where available, auxiliary dataset-internal identifiers (`cell_id_dummy`, `gnb_id_dummy`) can be used to associate a subset of NR measurements with inferred cell characteristics and estimated cell metadata. These identifiers are not standardized network identifiers and may be null.

Finally, users should be aware that the dataset reflects real-world drive-test conditions. Measurements may therefore include transient effects such as handover dynamics, beam switching, and short-term fluctuations in radio conditions. These characteristics make the dataset particularly suitable for data-driven and learning-based analyses but may require appropriate filtering or aggregation depending on the intended application.

Data Availability

The dataset is archived on Zenodo under concept DOI <https://doi.org/10.5281/zenodo.18322065>. This preprint describes version 3: <https://doi.org/10.5281/zenodo.18338399>.

Code Availability

Extensive in-house code was developed to parse, clean, and harmonize the raw Nemo Outdoor measurement logs. However, this code is highly project-specific and is not released as part of this dataset, since the processed data are provided in a ready-to-use format. The intention is to lower the entry barrier for researchers, including those without a strong telecommunications background. Consequently, users can work with the dataset directly without requiring access to the underlying post-processing scripts. Advanced users interested in the internal post-processing scripts may contact the authors directly to discuss potential access on a case-by-case basis.

Acknowledgements

The authors gratefully acknowledge Stadtvermessung Wien for providing building and terrain information of the city of Vienna, which forms an integral part of the DT included in this dataset.

References

1. Liu, Z. *et al.* *GenRadio: A Generative Framework for Fine-Grained 3D Radio Map Estimation in 2025 IEEE 102nd Vehicular Technology Conference (VTC2025-Fall)* (2025), 1–7.
2. Eller, L., Svoboda, P. & Rupp, M. A Deep Learning Network Planner: Propagation Modeling Using Real-World Measurements and a 3D City Model. *IEEE Access* **10**, 122182–122196 (2022).
3. Hoydis, J. *et al.* *Sionna RT: Differentiable Ray Tracing for Radio Propagation Modeling in 2023 IEEE Globecom Workshops (GC Wkshps)* (2023), 317–321.
4. Eller, L., Raida, V., Svoboda, P. & Rupp, M. Localizing Basestations From End-User Timing Advance Measurements. *IEEE Access* **10**, 5533–5544 (2022).
5. Ferrand, P., Guillaud, M., Studer, C. & Tirkkonen, O. Wireless Channel Charting: Theory, Practice, and Applications. *IEEE Communications Magazine* **61**, 124–130 (2023).

6. Zhang, Z., Peng, Z., Yu, H., Chen, M. & Liu, Y. Digital Network Twins for Next-Generation Wireless: Creation, Optimization, and Challenges. *IEEE Network*, 1–9 (2025).
7. Mussbah, M., Svoboda, P. & Rupp, M. *Statistical Analysis of Beam Dynamics in 5G Networks Using Drive-Test Measurements in 2025 IEEE Radio and Antenna Days of the Indian Ocean (RADIO)* (2025), 1–4.
8. Rochman, M. I., Ye, W., Zhang, Z.-L. & Ghosh, M. A Comprehensive Real-World Evaluation of 5G Improvements Over 4G in Low- and Mid-Bands. *IEEE Transactions on Cognitive Communications and Networking* **11**, 1427–1441 (2025).
9. Kousias, K. *et al.* A Large-Scale Dataset of 4G, NB-IoT, and 5G Non-Standalone Network Measurements. *IEEE Communications Magazine* **62**, 44–49 (2024).
10. Farthofer, S. *et al.* An Open Mobile Communications Drive Test Data Set and Its Use for Machine Learning. *IEEE Open Journal of the Communications Society* **3**, 1688–1701 (2022).
11. Yapar, Ç., Levie, R., Kutyniok, G. & Caire, G. Dataset of pathloss and ToA radio maps with localization application. *arXiv preprint arXiv:2212.11777* (2022).
12. Jaensch, F., Caire, G. & Demir, B. *Radio Map Estimation – An Open Dataset with Directive Transmitter Antennas and Initial Experiments* 2024. arXiv: 2402.00878 [cs.NI]. <https://arxiv.org/abs/2402.00878>.
13. Fastenbauer, A., Eller, L., Svoboda, P. & Rupp, M. *Comparison of Large-Scale Fading Models with RSRP Measurements in 2024 IEEE 99th Vehicular Technology Conference (VTC2024-Spring)* (2024), 1–6.
14. Caso, G. *et al.* The Chronicles of 5G Non-Standalone: An Empirical Analysis of Performance and Service Evolution. *IEEE Open Journal of the Communications Society* **5**, 7380–7399 (2024).
15. Miekkala, T. *et al.* *NordicDat: A Cross-Border Predictive QoS Dataset in GLOBECOM 2024 - 2024 IEEE Global Communications Conference* (2024), 1281–1286.
16. Schippers, H., Geis, M., Böcker, S. & Wietfeld, C. DoNext: An Open-Access Measurement Dataset for Machine Learning-Driven 5G Mobile Network Analysis. *IEEE Transactions on Machine Learning in Communications and Networking* **3**, 585–604 (2025).
17. Senderkataster. Accessed: 2024-11-18. <https://www.senderkataster.at/>.
18. ESRI GIS Dictionary. Accessed: 2025-08-27. <https://support.esri.com/en-us/gis-dictionary>.
19. Winncom Wireless Glossary. Accessed: 2025-08-27. <https://www.winncom.com/en/glossary>.
20. IBflex Datasheet. Accessed: 2025-09-16. <https://pctel.com/wp-content/uploads/2020/07/IBflex-Brochure-web.pdf>.